Facies (2006) 52: 265–278
DOI 10.1007/s10347-005-0032-2

ORIGINAL PAPER

Alain Préat · Salvatore Morano · Jean-Paul Loreau · Christophe Durlet · Bernard Mamet

Petrography and biosedimentology of the Rosso Ammonitico Veronese (middle-upper Jurassic, north-eastern Italy)

Received: 24 January 2005 / Accepted: 14 September 2005 / Published online: 22 February 2006

Abstract A petrographic and biosedimentological study of the *Rosso Ammonitico Veronese* from the Trento Plateau (north-eastern Italy) shows that diagenetic (neomorphism, recrystallization) and biological processes (microbial content and pigmentation) influenced the formation and alteration of the carbonate matrix. The subject of this article is the interaction of early diagenetic processes and an attempt to explain the different colors of the matrix (red, pink, grey). Nearly 200 samples derived from 14 sections (Callovian to Tithonian) located in the Verona area have been studied by means of classical, cathodoluminescence and SEM microscopy. Calcite and ferruginous microfilaments of different shapes and sizes are present and tentatively attributed to fungi and iron bacteria. These micro-organisms precipitated iron oxy-hydroxides at poorly dysoxic-anoxic sediment–water interfaces. Further liberation of submicronic hydroxides (now hematite) was responsible for the red pigmentation of the carbonate matrices, originally composed of less than 1 μm-sized micrite. Controversial smaller nanograins (0.1–0.5 μm) attributed to nanobacteria or planktonic picoeukaryotes have been observed in the reddish samples. Recrystallization of the micrite leads to the formation of new micritic crystals, between 2 and 4 μm in size, then to microspar crystals. Micritic textures are linked to the different colours of the samples. The intensity of the red colour is correlated with the presence of hematite (former iron hydroxides) and the presence of planar subhedral micritic grains. In contrast, pink and greyish samples are linked to the increasingly coalescent structure of anhedral micritic and microsparitic crystals.

A. Préat (✉) · B. Mamet
Département des Sciences de la Terre et de l'Environnement-Université Libre de Bruxelles. 50, avenue F. D. Roosevelt, CP, 160/02. 1050 Brussels, Belgium
e-mail: apreat@ulb.ac.be

S. Morano · J.-P. Loreau · C. Durlet
Centre des Sciences de la Terre, UMR CNRS 5561, 6 Bd Gabriel, 21000 Dijon, France

Keywords Rosso ammonitico · Bioprecipitation · Pigmentation · Diagenesis · Micrite · Jurassic

Introduction

The "Rosso Ammonitico Veronese" (RAV) is a Jurassic calcareous sedimentary stratigraphically condensed succession, formed by nodular limestones rich in ammonites (Martire 1996). It crops out in the Trento Plateau, in the Southern Alps (Fig. 1) and has been studied since the nineteenth century. De Zigno (1850) and Catullo (1853) published the first data on the red ammonite limestones from the surroundings of Verona. In more recent years, several paleontological, stratigraphic and sedimentological studies have been published (Sturani 1964; Clari et al. 1984; Sarti 1985, 1986, 1993; Martire 1988, 1989, 1992, 1996; Martire et al. 1991). None of these authors mentioned the existence of iron bacterial and fungal mats in the RAV carbonate matrix.

Recently the attention of some authors focused on the relationship between biosedimentological and petrographic features of the RAV. Clari and Martire (1996) studied the origin of the nodular structures so typical of this lithostrigraphic unit. They concluded that the formation of these structures is related to an early-localized cementation phase, which prevented the matrix from subsequent mechanical and intergranular compaction. Martire (1996) cited the presence of bacterial mats of unidentified origin without discussing their role. Scudeler-Baccelle and Nardi (1991) discovered amino acids in the carbonate concretions of the RAV nodular limestones (Upper Bajocian–Tithonian). Sethmann et al. (2001) reported three high values of fluorescence emission, due to the presence of recycled humic acids, responsible for metal accumulation, formation of oxides and direct precipitation of micrite. Mamet and Préat (2003) indicated the existence of bacterial filaments in the RAV sediments. They analysed 14 RAV sections and proposed that the origin of the pigmentation was linked to the activity of iron-oxidizing bacteria and fungi, originally localized at sediment–water interfaces

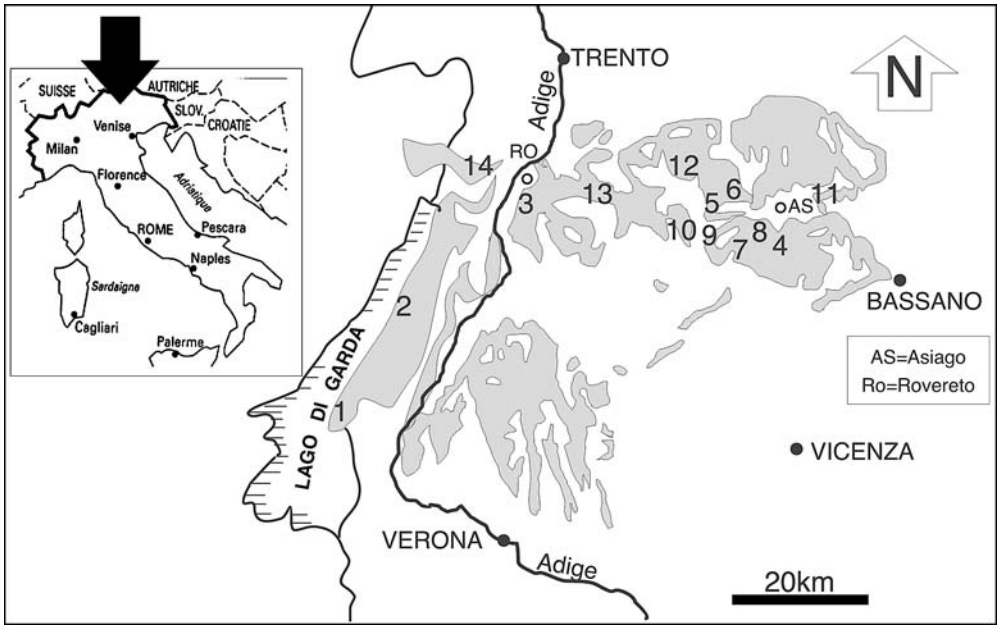

Fig. 1 Location of the 14 analysed sections (from Mamet and Préat 2003 and Sturani 1964, modified) in the Trento Plateau of the Southern Alps. (1) Acque Fredde 1 km south of Torri del Benaco, North of Gardo Lake. Description in Sturani (1964:11) (N 45°35.626, E 010°40.869). (2) Val di Sogno (Malcessine, km 80.1). Description in Sturani (1964:34) (N 45°44.751, E 010°47.935). (3) Roveretto, Ossario Castel Dante (between Madone del Campo and Ossario), Sturani (1964:16) (N 45°52.318, E 011°02.461). (4) Kaberlaba (active quarry, between Canove and Asiago, Martire (1996) (N 45°50.674, E 011°29. 275). (5) Mezzaselva (old quarry, entry of Mezzaselva (N 45°52.172, E 011°25.373). (6) Roana (new excavation at the entry of the village (N 45°52.534, E 011°27.289). (7) Ponte Guelpach (Canove road, direction Vicenza). Description in Sturani (1964 p. 28) (N 45°51.183, E 011°27.374). (8) Voltascura (large active quarry near Ponte Guelpach. Martire (1996) (N 45°50.905, E 011°27.249). (9) Rabeskini (old quarry and outcrop). Martire (1996) (N 45°51.845, E 011°26.307). (10) Castelletto (exit of the village, curve no 16). Martire (1996) (N 45°51.334, E 011°22.466). (11) Chapel of San Sisto (old quarry near the chapel, close to Asiago) (N 45°51.266, E 011°30.930). (12) Forte di Campo Luserna (abandoned fort, altitude 1546 m). Description in Sturani (1964:19) (N 45°55.605, E 010°20.174). (13) Serrada. Outside the village, large curve along the road to Terragnolo (N 45°53.271, E 011°09.074). (14) Ceniga. Natural outcrop at the exit of the village (N 45°56.968, E 010°54.314)

in poorly oxygenated marine environments. The red pigmentation was linked to the accumulation and dispersion of submicronic iron hydroxides in the micritic matrix.

The aim of this work was to determine how microbial activity interacted with the biomineralization and carbonate diagenesis of the RAV series. The facies are varied and show evidence of early lithification near the sediment–water interface (Clari and Martire 1996). The following questions will be investigated: (a) Are microbes linked to initial formation or diagenesis of the matrix? (b) Is the microbial content the same for different micritic textures and pigmentations? (c) What is the diagenetic chronology? (d) When does the micritic pigmentation originate?

Geological setting and stratigraphy

The RAV is a condensed sedimentary succession of Late Bajocian to Tithonian age. It is mainly composed of reddish nodular limestones, deposited on the distal "Trento Plateau" (Gaetani 1975; Bosellini and Martinucci 1975; Bosellini and Winterer 1975; Winterer and Bosellini 1981) located in the southern continental margin of the Tethyan Ocean. This paleogeographic unit was a structural high until the late Early Jurassic. Successive platform drownings led to pelagic carbonate sedimentation (Zempolich 1993). So the RAV marked the change from shallow water to pelagic carbonate sedimentation. This submarine plateau was delimited by deeper basins (Lombardian basin and Belluno Trough) (Fig. 2). Typical RAV features are the presence of hardgrounds, highlighted by Fe and Mn oxide encrustations and recording breaks in sedimentation (Clari et al. 1984; Martire 1989), colour variations, abundance of nodular facies and bioturbation.

In the Verona area, the RAV is less than 30-m thick and it is subdivided into three units and eight different facies (pseudonodular, mineralized, bioclastic, nodular, thin-bedded limestone, thin-bedded cherty limestone, subnodular, stromatolitic) (Martire 1992, 1996; Clari and Martire 1996) (Fig. 3) The lowest unit, the "Rosso Ammonitico Inferiore" or RAI (Upper Bajocian–Lower Callovian) is formed by pseudonodular, mineralized and massive facies; the middle unit, the "Rosso Ammonitico Medio" or RAM (Upper Callovian–Middle Oxfordian) is formed by thin bedded**,** cherty and subnodular limestones; the upper unit, the "Rosso Ammonitico Superiore" or RAS (Lower Kimmeridgian–Upper Tithonian) is composed of stromatolitic, pseudonodular and nodular limestones. The pseudonodular facies (RAI) consists of wackestones with bivalves (*Bositra*), planktonic and benthic foraminifers (*Protoglobigerina*, *Lenticulina*), ostracods, radiolarians and peloids. The bioclastic facies are

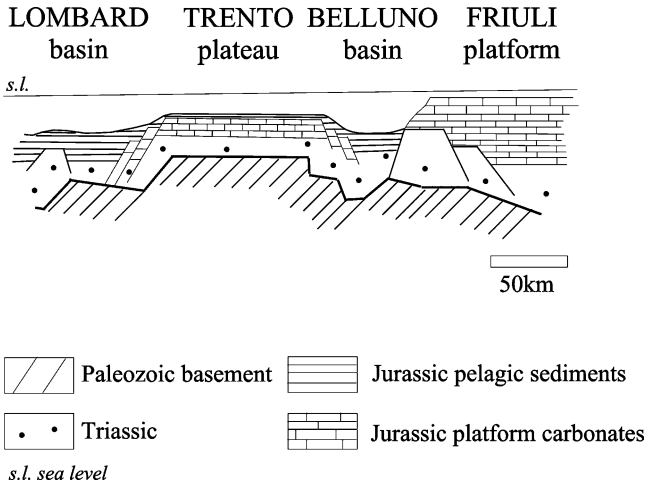

Fig. 2 Paleogeographic sketch of the western Tethys during late Jurassic, modified from Caracuel et al. (1997)

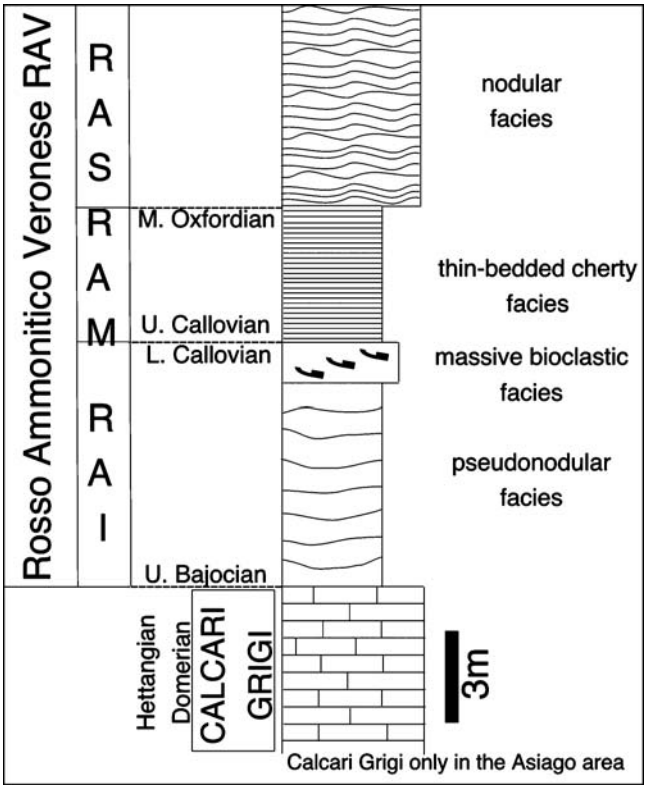

Fig. 3 Stratigraphy of the Rosso Ammonitico Veronese (modified from Martire 1996): RAI = Rosso Ammonitico Inferiore (lower); RAM = Rosso Ammonitico Medio (middle); RAS = Rosso Ammonitico Superiore (upper). The underlying 'Calcari Grigi' is restricted to the Asiago area

formed by peloidal packstones and rare grainstones with bivalves and crinoids. The thin-bedded facies (RAM) consists of red chert lenses and are represented by bivalve wackestones–packstones and mudstones with radiolarian moulds. The nodular facies (RAS) consists of bioclastic packstones with bivalves, foraminifers and crinoids.

In the Altopiano di Asiago area the RAV rests unconformably on the 600-m thick Liassic (Domerian) shallow-water "Calcari Grigi" Formation with a large stratigraphic gap (Aalenian to Late Bajocian). In its upper boundary, the RAV gradually grades to the white Cretaceous Maiolica Limestone. Bivalve- and ammonite-bearing coquinas are locally present at the top of the "Calcari Grigi", mainly as fillings of cavities (Sturani 1971; Winterer et al. 1991; Martire 1996). This level, known as Lumachella a *Posidonia alpina* is Early to Late Bajocian age (Sturani 1971).

Material and methods

Analytical procedures

About 200 samples, derived from 14 sections (Mamet and Préat 2003) have been analysed. The sections are located in north-eastern Italy, close to the Lake of Garda and the towns of Asiago and Rovereto (Fig. 1).

The methodology for this study included complementary biosedimentological, diagenetic and geochemical approaches. First, samples were subdivided into three classes, according to color (red, pink and grey). Each class was analysed by means of classical, cathodoluminescence (Techosyn 8200 MKII) and SEM (JSM 6400 scanning microscope) miscrocopy in order to find what relationship, if any, exists between sample colour and petrographic features. In addition, chemical ($CaCO_3$, Mg, Mn, Fe, and Sr contents) and stable isotope (^{13}C,^{18}O) analyses on samples from the Voltascura and Forte di Campo Luserna sections, were carried out. Trace element analyses (University of Burgundy, Dijon) were carried out according to the following procedure: sample powders were attacked in acetic acid under cold temperature conditions, in order to separate soluble carbonate from insoluble phases. After filtration, the acid solution was submitted to a double hydrochloric acid leaching: the first, to eliminate the acetates and the second, to change the medium to HCl more appropriate for the Atomic Absorption Spectrometry. Finally, solutions were brought to a constant calcium content level (Ca=2500 ppm kg^{-1}). The stable isotope analyses (by Dr M Joachimski, University of Erlangen) were performed on 24 red, pink and grey samples as follows: carbonate powders (10–15 mg) were attacked with 100% phosphoric acid (density >1.9, Wachter and Hayes 1985) at 75°C using a Kiel III online carbonate preparation line connected to a ThermoFinnigan 252 masspectrometer. All values are reported in per-mil relative to V-PDB by assigning a $\delta^{13}C$ value of +1.95‰ and a $\delta^{18}O$ value of −2.20‰ to NBS19.

Colour evaluation

As the colour of the samples is an important discrimination factor in our study one should mention the following observations.

1. 'Red' samples have been collected in all RAI and RAS facies (the RAM facies have not been considered), i.e., the pseudonodular, mineralized, bioclastic, stromatolitic

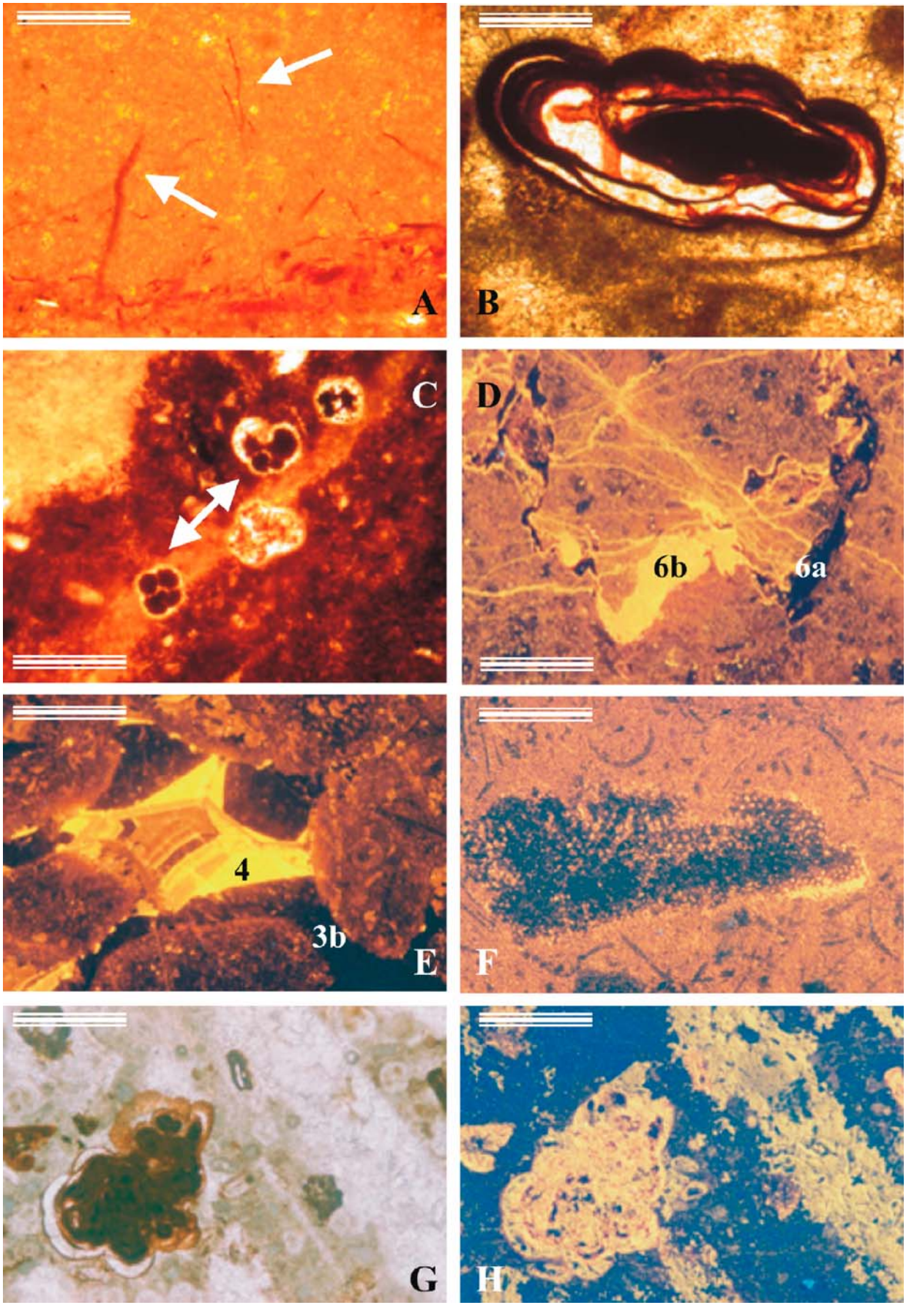
A
B
C
D
6b
6a
4
3b
E
F
G
H

and nodular facies. The dominant pigmentation is red from homogeneous to heterogeneous at a centimetric scale.

- the heterogeneous pigmentation is typical of the pseudonodular and nodular facies displaying different colours from pinkish to brick red. This could be attributed to slight bioturbation as revealed under the microscope (sample AR50);
- the red homogeneous pigmentation is typical of stromatolitic facies. These latter consist of finely laminated peloidal boundstones (stromatolitic domes and oncoids) with Fe-oxides accumulation between the laminae (samples AR72, 139). The bioturbation is absent. These oncolites and stromatolites can also constitute the nodules of the pseudonodular facies (sample AR119);
- the mineralized facies contains varied dark brown mineralized grains (intraclasts sensu Martire (1996); 'blebs' sensu Mamet and Préat (2003)) in a homogeneous red or pinkish matrix (samples AR13, 57, 69). The bioturbation is nearly absent and the facies is a pelleted packstone with undisturbed laminations of thin pelecypod shells. The matrix can also be greyish to yellowish (sample AR74);
- the bioclastic facies is a greyish or reddish packstone or grainstone with abundant pelecypods and echinoderms. The colour distribution is highly heterogeneous in the greyish facies (sample AR122) or more homogeneous in the red ones (samples AR145, 146, 150). White and grey facies are typical of the Lumachella a *Posidonia alpina* (crinoidal grainstone) at the top of the 'Calcare Grigi' (sample AR106).

2. The primary objective of this paper is to see if red (and pink) facies and non-red facies (white and grey) are microbialites or not. Thus the selected samples were chosen on the base of their colour homogeneity. The best-retained red samples come from the stromatolites in the pseudonodular or in the stromatolitic facies and from the mineralized stromatolites in the more homogeneous mineralized facies. These particularly homogeneous samples often display a clotted peloidal matrix. The grey and white samples were chosen in the more homogeneous facies of the molluscan and echinodermal grainstones of the top of the 'Calcari Grigi' and also in the RAI.
3. Selected samples. Around 200 samples have been collected and studied from thin sections. The samples used in this paper are the followings (geographical location in Fig. 1):

AR1, 2, 4, Acque Fredde, nodular facies, RAS, red brick (homogeneous);
AR13, Val di Sogno, nodular facies, red (homogeneous);
AR50, Kaberlaba, RAI, pseudonodular facies, pink-red (heterogeneous):
AR57, Mezzaselva, pseudonodular facies, RAS, pink-red (homogeneous);
AR69, 72, Roanna, nodular facies, RAS, red (homogeneous with stromatolitic lamination in AR72);
AR83, 84, 85, 87, 88, 90, 91, 92, 93, 95, 97, 100, 102, 106, 115, 116, 117, Voltascura, mineralized (83–93, 115–117), pseudonodular (95–97), 'Lumachella a *Posidonia alpina*' (100–106), RAI, all reds except 100–106 which are grey (heterogeneous),
AR119, 122 Rabeskini, pseudonodular facies, RAS, pinkish (stromatolitic and homogeneous 119, reddish heterogeneous 122);
AR135, 139 Castelletto, pseudonodular facies (139 is stromatolitic), RAS, red;
AR145, San Sisto, bioclastic facies, RAI, pinkish–reddish;
AR146, 147, 148, 150, 151, 156, 160, 161, 162, Forte di Campo Luserna, pseudonodular facies, RAI, red (homogeneous) except 148 (pink) and 160-161 'Calcari Grigi' (grey).

Fig. 4 **A** Bacterial and fungal filaments associated to thin hardground into red matrix (Ar102, Voltascura section, scale bar 40 μm). **B** Oncolitic-microstromatolite with manganese, iron and calcite layers (sample Ar119, Rabeskini section; Upper RAI, 2 metres below the RAS member, scale bar 40 μm). **C** *Protoglobigerina* with iron and manganese infillings (sample Ar139, Castelletto section, RAS member, scale bar 40 μm). **D** Stylolite with non-luminescent cement (phase 6a) and yellow luminescent cement (phase 6b) in dull-orange matrix (phase 5) (sample Ar146, Forte di Campo Luserna section, RAI member, scale bar 100 μm). **E** Crinoidal grainstone under cathodoluminescence (sample Ar150, Forte di Campo Luserna section, RAI member). Chronology of calcite cements: 3b nonluminescent cement; 4 high luminescent yellow cement; 5 dull-zoned luminescent orange cement. Scale bar 40 μm. **F** Bivalve (*Bositra*) and echinodermal wackestone under cathodoluminescence showing phases 3b-4-5 (see text) (sample Ar50, Kaberlaba section, RAI member, scale bar 100 μm). **G,H** Oncolitic-microstromatolite similar to Fig. 2 with calcite and manganese layers under classical microscopy (Fig. 9G) and cathodoluminescence (Fig. 9H). Figure 7 shows partial dissolution of former Fe–Mn layers. The microstromatolite is characterized by a luminescent yellow cement similar to the luminescence of the nearby fracture, and does not affect the non-luminescent cement. Sample Ar122, observed, Upper RAI member, Rabeskini section, scale bars 100 μm

Results

Petrographic data

Red samples

Red samples analysed under classical microscopy show some distinctive features. Red micritic matrices (foraminiferal mudstones-wackestones, oncolitic-microstromatolite wackestones and bivalve packstones), often presenting a clotted fabric, are not or only slightly bioturbated. These red matrices display four different homogeneous fabrics: (i) dense micrite, (ii) 'peloidal' clotted, (iii) finely laminar [stromatolites] and (iv) fine microspar. These matrices are slightly to moderately bioturbated and the resulting burrows have small to minute diameters. The more evident burrows have diameters varying between

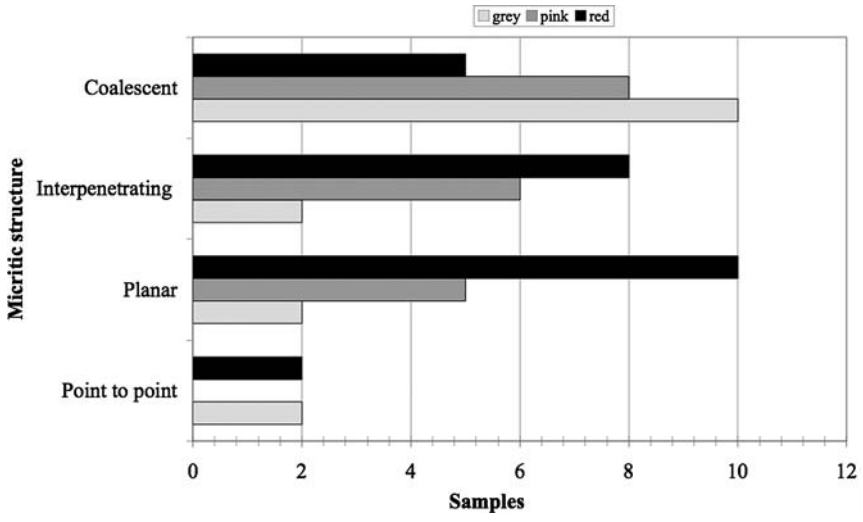

Fig. 5 Micritic structures for red, pink and grey samples under SEM microscopy. Horizontal axis shows the number of analysed samples for each colour class

0.3–0.5 mm and lengths less than 1 mm to a few millimetres (up to 2 mm) and resemble to the ichnospecies *Chondrites* (Bromley 1990). Their density rarely exceeds 10% (eye estimation).

The red matrices contain numerous fragile microfilaments attributed to iron-oxidizing bacteria and fungi. They would have been destroyed, should the burrowing be intense. According to their disposition, shape and size, these microbes have been classified by Mamet and Préat (2003) in several types, ranging from straight to dichotomic forms. These bacterial and fungal filaments are present in mudstones (Fig. 4A), where they are also associated with thin hardground horizons. Other peculiar features are the presence of bioclasts with hematite infillings (Fig. 4C) and oncolitic-microstromatolites formed by alternation of calcite, Fe- and Mn-oxides layers (Fig. 4B, G, H).

SEM analysis (up to 30.000×) showed that micrite is characterized by abundant planar nanostructures (with grains in contact through their surfaces), abundant subhedral morphologies and sizes ranging from 0.1 to 4 μm. Sometimes point-to-point micritic contacts are evident (Figs. 5 and 6). This micrite is composed of coccoliths, nanobioclasts and unidentified fossil fragments. Smaller micritic grains (<1 μm) are mixed with the nanobioclasts and are included in larger micritic and microsparitic grains with an euhedral morphology (more crystalline faces are visible) and point-to-point grain contacts (Fig. 7C). These larger micritic grains range from 2 to 4 μm, show subhedral amoeboidal morphologies, interpenetrating textures and form an incipient neomicrite ('pseudo-cement') sensu Loreau (1972). A homogeneous 'clear' microspar (>4 μm), with dominant interpenetrating textures and anhedral or subhedral morphologies is also associated but never abundant.

Pink samples

The petrographic features of pink samples are generally comparable with those of the reddish ones, although some differences can be emphasized: pink matrices show fewer iron bacterial filaments and are slightly bioturbated. In addition, bioclasts are not completely filled or surrounded by iron oxides as observed for the red samples. At SEM magnification, micrite indicates the presence of coalescent structures and subhedral morphologies (Figs. 5,6, 8A). As in the red samples, neomicrite shows interpenetrating structures and amoeboidal morphologies. It still encloses the smallest rounded micritic grains (<1 μm), which appear to be lined up, at the boundaries and cleavages of crystals (Fig. 8C, D). Microspar crystals are more coalescent than in the red samples (Fig. 8A, E). The microstratigraphic chronology of red samples is also recognizable.

Grey samples

In thin section, grey samples consist of peloidal bioclastic packstones and rare ooidal grainstones. This facies is strongly burrowed. Iron bacterial filaments and bioclasts with hematite infillings are lacking. At SEM analysis, micrite rarely shows fabrics with point-to-point contacts. Micritic matrix, as well as neomicrite, also indicates the predominance of coalescent structures and anhedral grain morphologies (only one face of crystals is recognizable) (Figs. 5,6,8F).

There are no organic network or iron bacterial and fungal filaments recognizable on the micritic support. The smallest micritic grains (<1 μm) are rarely recorded. Microspar is relatively more abundant than in reddish samples and shows larger coalescent structures and anhedral morphologies.

Microstratigraphy of the petrographic phases

SEM and cathodoluminescence analyses permit the establishment of the chronology of the successive phases in the different coloured matrices (Fig. 9):

(1) Initial phases
(1a) This phase is represented by coccoliths (Fig. 7B), nanobioclasts and unidentified fossil fragments;

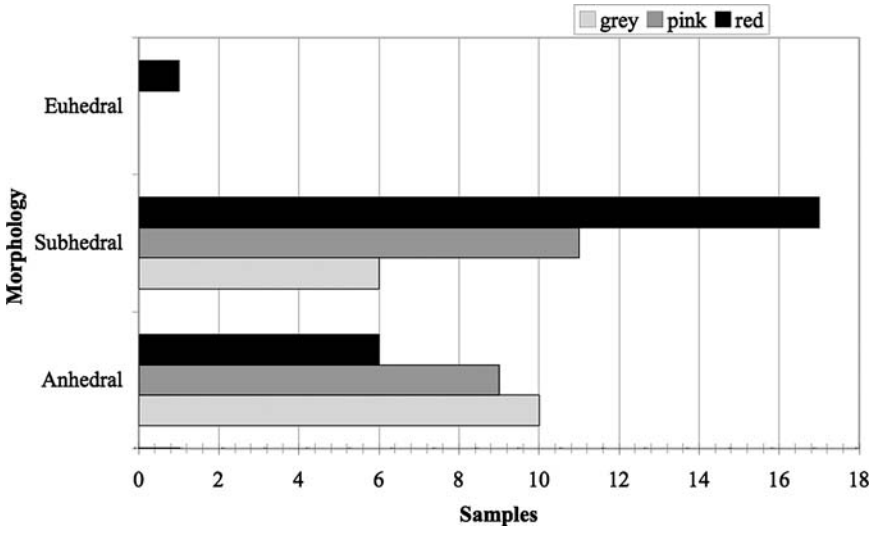

Fig. 6 Morphology of micrite for red, pink and grey samples under SEM microscopy. Horizontal axis shows the number of analysed samples for each colour class

(1b) This phase refers to the smallest micritic grains in the whole compositional pattern. Micritic grains with a size less than 1 micron are mixed with nanobioclasts (phase 1a) and included in larger micritic and microsparitic grains, belonging to successive diagenetic phases (phases 2 and 3). These small-sized grains probably represented the initial micritic record of the carbonate sedimentation, when micrite was still not affected by successive neomorphic growth (Fig. 7A, B). The open question is to know if this initial small-sized micrite was chemically precipitated, or was represented by calcified nanobacteria (sensu Folk 1999) or planktonic picoeukaryotes (Courties et al. 1994; Van Den Hoek et al. 1995). At this step the intergranular nanoporosity is relatively high;

(1c) The former small-sized micritic support (phases 1a–1b) was colonized by iron-oxidizing bacterial and fungal hyphae, forming mats within the carbonate matrix (Fig. 7E). At this step, the microbial activity led to the bioprecipitation of submicronic iron/manganese oxy-hydroxide minerals in the reddish facies at dysoxic–anoxic water interfaces. Since these microbes were probably growing under microaerophilic conditions, autooxidation of Fe^{2+} is to be expected to proceed at slow rates (Ghiorse 1984). In these conditions bacteria oxidized passively the ferrous iron (Brierley 1990). This has already been suggested for various Devonian limestones (Préat et al. 1999; Boulvain et al. 2001).

(2) First matrix recrystallization characterizes the next three steps

(2a) This phase is related to the development of an incipient neomicrite ('pseudo-cement'), filling the original intergranular nanoporosity. During this stage the previous ferruginous filaments were destroyed and liberated submicronic oxy-hydroxides in the matrix. It is during this stage that micrite still shows euhedral morphology and point-to-point grain contacts (Fig. 7C);

(2b) The recrystallization process continued producing larger micritic grains, with a size ranging between 2 and 4 μm. They show subhedral amoeboidal morphologies and interpenetrating textures with inclusions of smaller rounded and lengthened calcitic grains (Fig. 7C, D), which might represent relics of phase 1a and/or remains of nanobacteria;

(2c) Some of the largest microbial filaments are still preserved and form an organic network that occurs at the compromise boundaries of the crystals (Phase 2c, Fig. 8B).

(3–6) Further successive growth of crystals beyond 4 μm forms homogeneous microspar, with dominant interpenetrating textures and anhedral or subhedral morphologies (Fig. 7A, phase 3). The residual pores are progressively filled with further calcite cements, respectively nonluminescent (phase 3b, Fig. 4E); luminescent (phase 4, Fig. 4E) and dull luminescent (phase 5, Fig. 4E). Pressure-dissolution features are underlined by stylolites (phase 6a, Fig. 4D). The last step consists of fractures filled with a luminescent cement (phase 6b, Fig. 4D). The microspar phase (3) is poorly developed in the red samples. In the grey samples, this chronological sequence of diagenetic phases significantly differs from that of the reddish samples. Here the initial phase, represented by a small-sized micrite (phase 1b), passes directly to a microspar phase (phase 3), without going through the intermediate steps (phases 1c to 2c).

Diagenetic stratigraphy

About 50 red, pink and grey samples have been analysed by cathodoluminescence. Bioclasts, micritic matrix and calcite cements show zones with different luminescent intensities.

One of the most important observations is that micrite (whatever the sample colour) displays a dull luminescence, with a typical orange colour (Fig. 4F). A non-luminescent intragranular cement is associated with *Bositra* shells, echinoderms, and intergranular syntaxial crinoidal

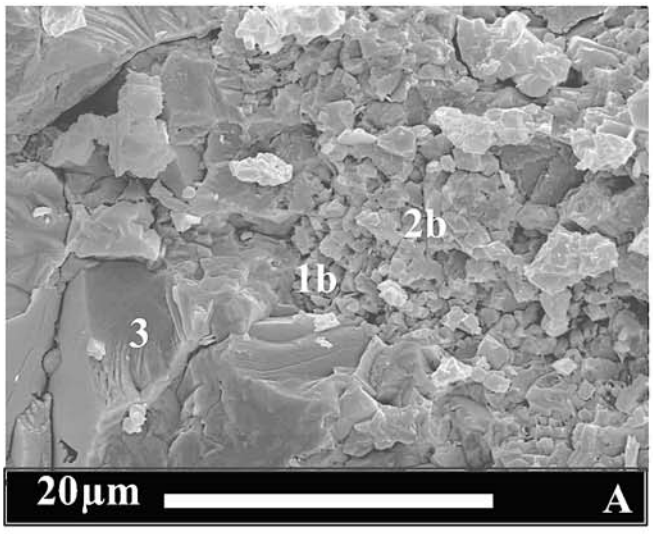
2b
1b
3
20µm
A

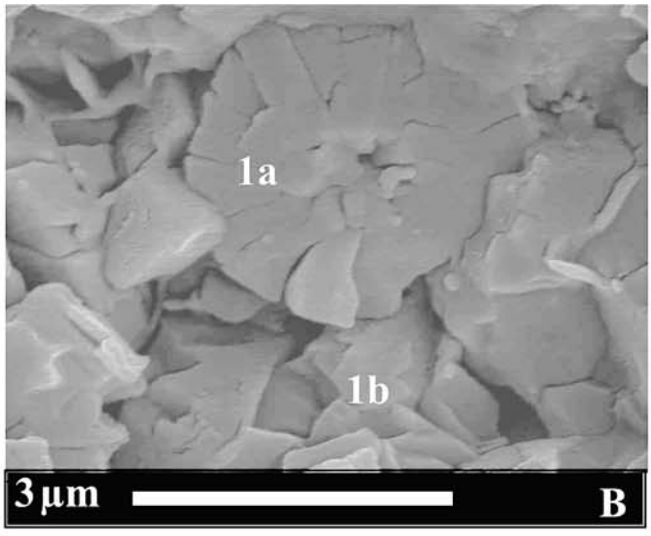
1a
1b
3µm
B

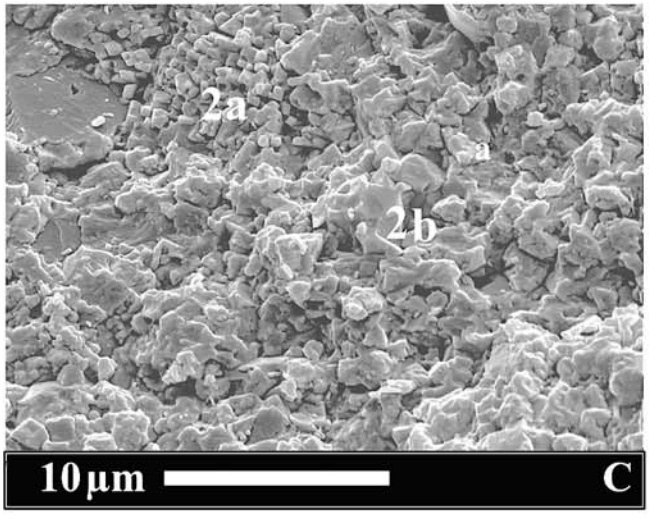
2a
a
2b
10µm
C

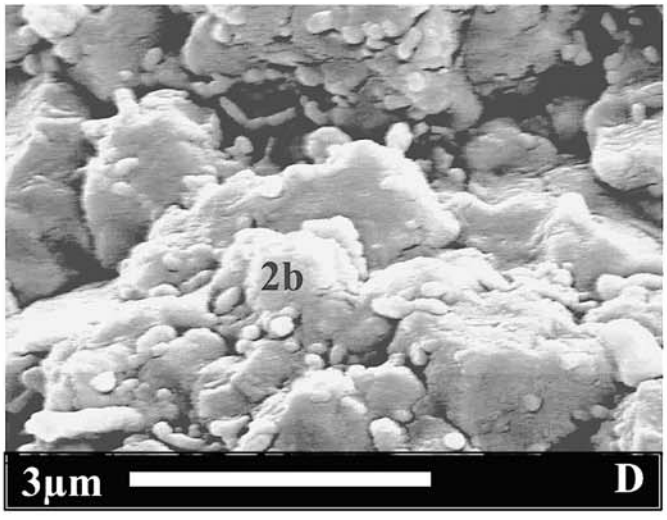
2b
3µm
D

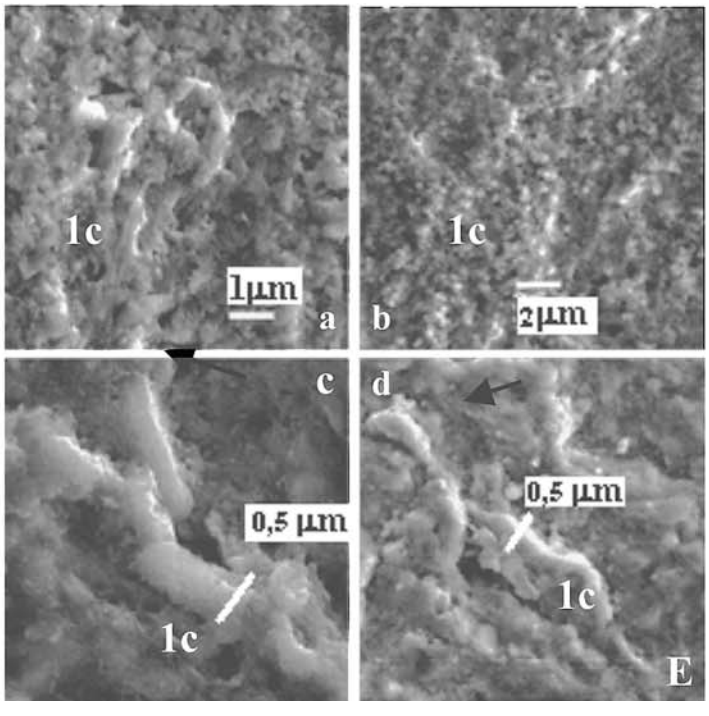
1c
1µm
a
1c
b
2µm
c
0,5 µm
1c
d
0,5 µm
1c
E

overgrowths (Fig. 4E, F, phase 3b). This non-luminescent phase is also characteristic of the microspar and is easily recognizable. Slightly luminescent subzones are irregularly distributed in this phase. Luminescent yellow intergranular cement developed on the non-luminescent one (Fig. 4E, phase 4). This cement is present on the outer parts of syntaxial crinoid overgrowths, in the calcite layers of Fe–Mn oncolitic-microstromatolites, as well as in the cavities of dissolved shells. In particular, oncolitic-microstromatolites display this luminescent cement which is also observed in the associated microfractures. As the former non-luminescent cement phase, the yellow cement is weakly zoned. A dull orange luminescent cement fills the residual intergranular porosity or the intragranular dissolved bioclast cavities, and also characterizes the micritic matrix (Fig. 4E, F). This cement is present in the micritic bioclast alterations. A late non-luminescent cement is associated with stylolites (Fig. 4D, phase 6a), while a high luminescent cement fills larger fractures and veins which are overprinted on stylolites (Fig. 4D, phase 6b).

The relationships between cement phases suggest the following chronology:

- Non-luminescent intragranular and intergranular cements (phase 3b) indicate an oxic or suboxic environment without oxygen gradients (Machel 1999) in the grey facies and oxic-dysoxic sediment–water interfaces in the red facies where oxygen levels decreased. In these latter facies ferrous iron was oxidized by iron bacteria. This type of process has been previously reported by Fenchel and Finlay (1995).
- The luminescent yellow cement belongs to phase 4 and records the transition of dysoxic to anoxic interfaces in the red facies, where oxygen levels continued to decrease, or increasingly reducing environments in the grey facies due to burial. Non-enzymatic and/or enzymatic reduction of the former oxidized manganese (Mn^{4+}) of phase 1 was probably significant in these microenvironments (Aller 1990). Luminescence inside calcite microstromatolites reveals the importance of the manganese dissolution (Mn^{2+}) from its previous oxidized state (Mn^{4+}) (Megonigal et al. 2003). This increase of reducing conditions during burial diagenesis is characteristic of the red facies. Dissolution is also highlighted by associated luminescent calcite veins. Dissolution occurred in a closed system since the non-luminescent cement outside oncolitic–microstromatolites was weakly or not at all affected (Fig. 4B, G, H).
- Dull luminescent orange calcite cement (phase 5) is the latest pore-filling cement in the zoned cements. It is sometimes subzoned from dull orange to dull brown. It is frequently associated with beds lacking intense pressure solution and/or extensive breakage of shells (*Bositra*). This suggests that this facies had been partially cemented by dull cements which formed under shallow burial conditions as indicated by the weak overburden of the series (700 m in Clari and Martire 1996)
- Non-luminescent cement (phase 6) related to chemical compaction (stylolites) and final highly luminescent calcite (fractures) terminate the diagenetic sequence.

◀ **Fig. 7** **A** Phase 1b: micrite; Phase 2b: neomicrite; Phase 3: microspar. Ar1, Acque Fredde section, RAS member. **B** Phases 1a (coccolith) and 1b (smallest micritic grains). Ar69, Roana section, RAS member. **C** Phase 2a: incipient neomicrite; phase 2b: neomicrite. Ar2, Acque Fredde section, RAS member. **D** Neomicrite (Phase 2b) showing interpenetrating structure and subhedral morphology. Black arrows: nanobacteria? enclosed in neomicrite and showing size less than 1 μm. Ar4, Acque Fredde section, RAS member. **E** Phase 1c: Iron oxidizing bacterial filaments on small-sized micrite. They are neither fungi because they are much smaller than typical fungi, nor cyanobacteria because they are coated by iron. Ar135, Castelletto section, RAI member

Geochemistry

The results of chemical analyses on 25 samples from the Voltascura and Forte di Campo Luserna sections are summarized in Table 1 and Figs. 10 and 11. They give the percentages of $CaCO_3$ and Mg, Fe, Mn, Sr contents (ppm). Analyses show that the iron content is generally low. Whatever the colour of the facies, the Fe (and Mn) contents present small values: <350 ppm of Fe in the red and grey facies. Low iron contents are also observed in Frasnian red mud mounds from Belgium (Boulvain 1993). The only somewhat high concentrations are always related to the presence of post-sedimentation stylolites. By comparison with percentages the quantities are much smaller (by a factor of 10) as those observed in comparable sedimentary grey or blackish successions in the Mid Devonian of Belgium (Préat et al. 1983). The absolute iron content is therefore not the origin of the pigmentation, but the mineralogy explains the colour of the limestones: the iron is present as Fe^{2+} in the calcite lattice in the grey facies and as submicronic hematite (from former oxy-hydroxides produced by microbial activity) in the red facies. The Mn content is also comparable in the different facies (up to 1387 ppm in the grey facies) and does not correlate with the iron content. The manganese has been remobilized (diagenetic phase 4) during early diagenesis in a closed system. The very low Sr content (generally 50–100 ppm) suggests that no aragonitic precursor or aragonite was ever present. Bacterial activity, producing exchanges of CO_2 (respiration, oxidation of ferrous ions) in the microenvironment probably led to quick transformation of HMC and aragonite in LMC (Hendry 1993; Tobin and Walker 1996) with less than 3500 ppm Mg (Table 1). That was one of the first possible diagenetic change, perhaps induced by the presence of bacteria, provoking an early carbonate mineralogical stabilization in the red facies. The grey facies were later stabilized during increasing burial, possibly by dissolved calcium carbonate coming from the ammonite molds which are locally abundant (Clari and Martire 1996) and could have provided the 'cement' of the microspar following the process described by Munnecke et al. (1997).

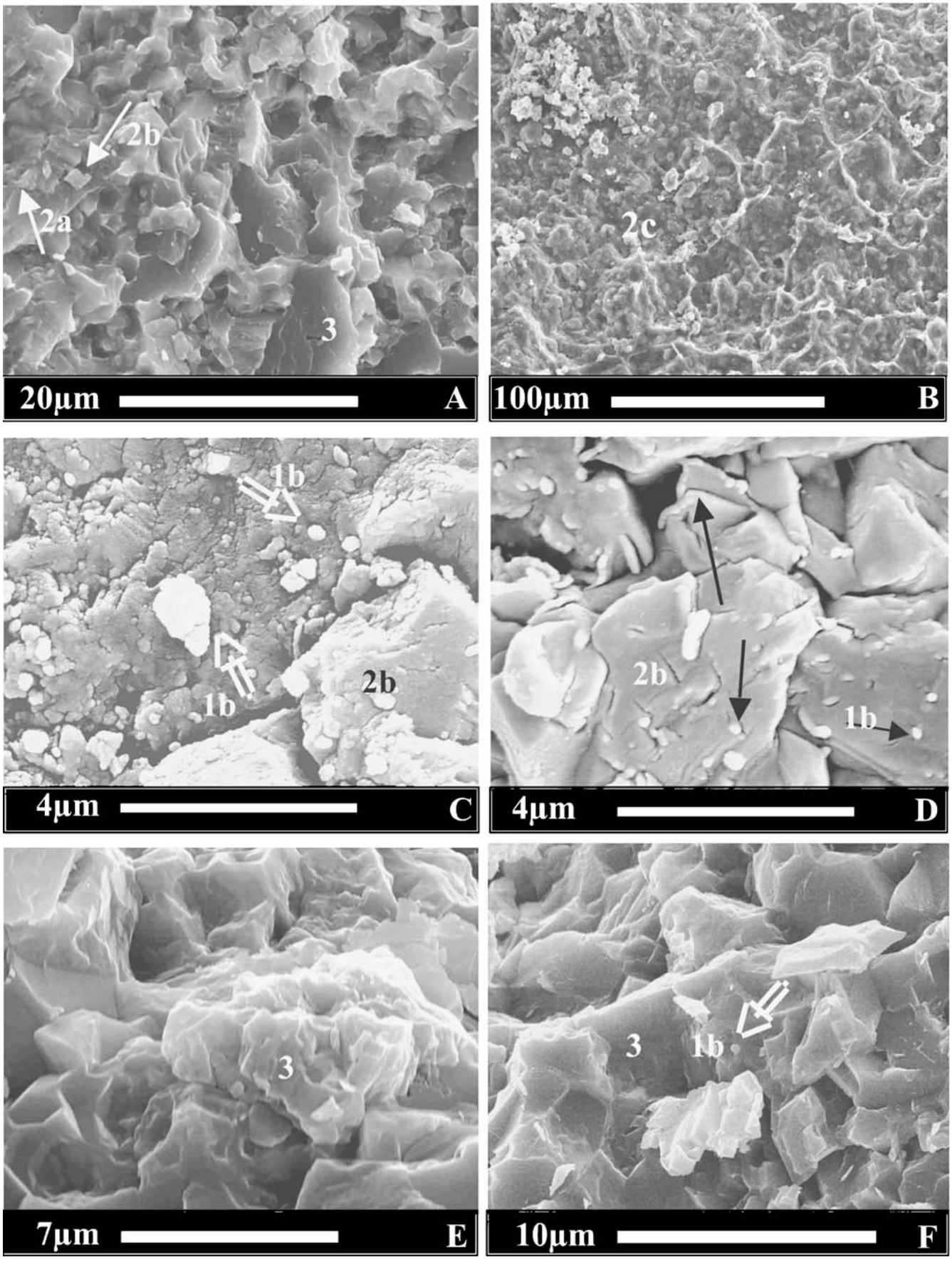
2b
2a
3
20µm
A
2c
100µm
B
1b
1b
2b
4µm
C
2b
1b
4µm
D
3
7µm
E
3
1b
10µm
F

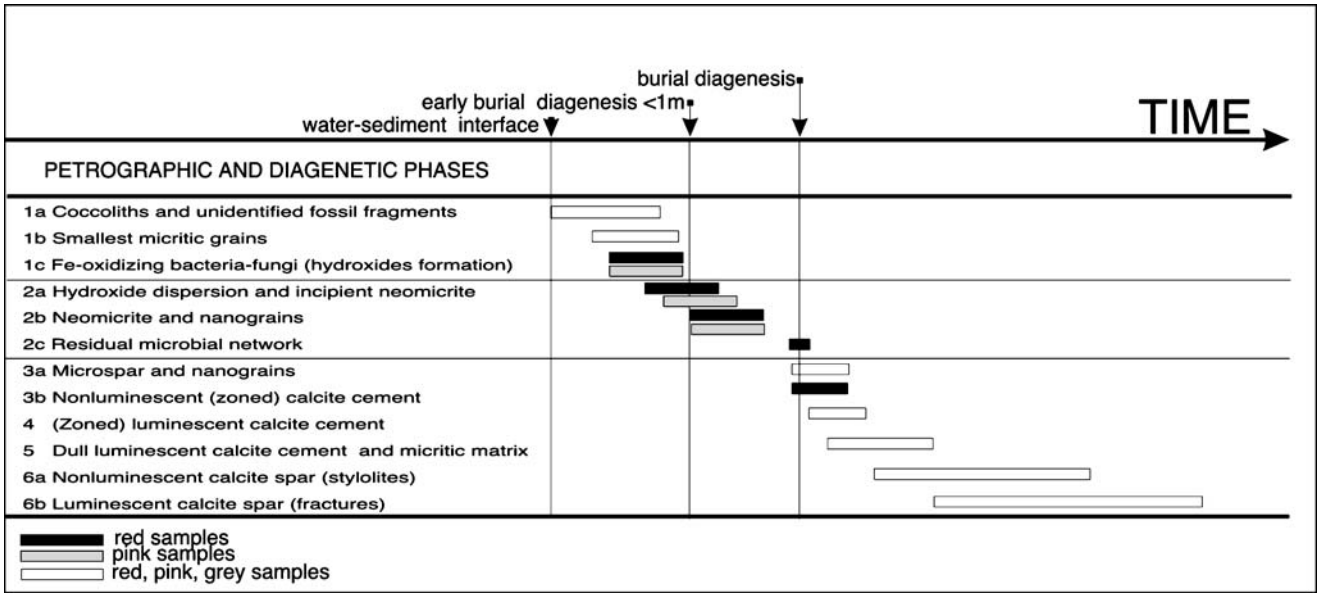

Fig. 9 Paragenetic sequence summarizing chronology for different sedimentary and diagenetic phases

The stable isotope analyses give evidence that there are no important differences between the $\delta^{13}C$ values of the two sections and differently coloured samples. The values range from +2.0 to +3.2‰ $\delta^{13}C$ and match the marine values reported for Early Jurassic times (Jenkyns and Clayton 1986). Most of $\delta^{18}O$ values are near the marine signature of Early Jurassic times indicating that no meteoric water has been involved in the diagenesis. The slighty more negative values of Voltascura ($\geq$1‰) could indicate that the temperature was slightly higher than in the Forte di Campo Luserna area ($\leq$1 ‰). This indicates that differential subsidence and burial rate occurred during this time. This fits the general structural framework of faulted blocks of the Altopiano di Asiago during the Late Callovian (Martire 1996).

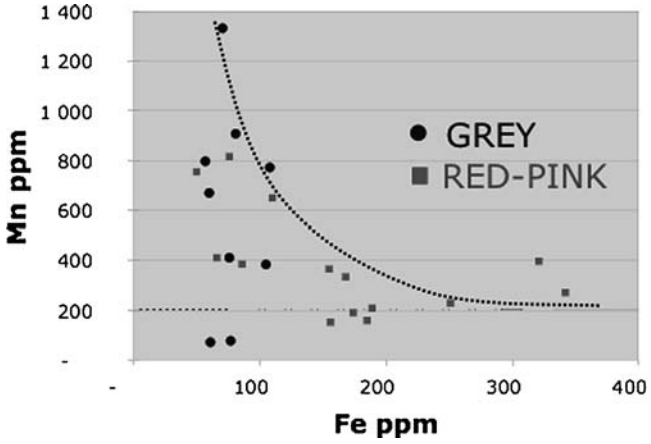

Fig. 10 Fe vs. Mn contents from the Voltascura and Forte di Campo Luserna sections (see Table 1)

The problem of bioturbation

If we consider clayey micritic sediment and water (i.e. our facies) as macrohabitats, we have to recognize that the effective habitats for micro-organisms are microhabitats or 'microenvironments' (Stolp 1988). Marine sediments represent highly complex ecosystems. Compared to laboratory cultures, microbes in Nature live in a heterogeneous environments influencing uptake of nutrients and metabolic activities. Local changes (e.g., redox potential and pH) vary over short distances (Stolp 1988; Schulz 2000; Munn 2004). The effects are drastic with respect to O_2 conditions and the diffusion of oxygen into the sediments is extremely low. This does not mean that bioturbation is impossible: in modern seas the meiofauna [e.g. size of about 0.1 to a few mm] (especially nematodes, turbellaria, gnathostomulids and gastrotrichs) thrive in sediments with a very low p_{O_2}, and may live permanently under anaerobic conditions (Fenchel and Finlay 1995).

Small species (and nematodes with a very small diameter) dominate 'dysaerobic' habitats in sediments. The small size of these organisms means that they can function as aerobes with oxygen tensions around or below the detection limit (Powell 1989). Most of this fauna is found above the sulphidic zone in the suboxic zone. This layer may be

Fig. 8 **A** Phase 2a (white arrow, incipient neomicrite); Phase 2b (black arrow, neomicrite) and Phase 3, microspar showing anhedral structure and coalescent morphology. Ar13, Acque Fredde section, RAS member. **B** Phase 2c: microbial filaments occurring as organic network at the compromise boundaries of neomicritic crystals. Ar74, Roana section, RAS member. **C** Phase 1b (arrow), Phases 2b and 3. Ar100, Voltascura section, top of the "Calcari Grigi", near the contact with the RAI member. **D** Phases 1b and 2b: neomicrite with interpenetrating structure and subhedral morphology; black arrows: nanobacteria? enclosed into neomicrite and lined up on crystal boundaries. Ar145, San Sisto section RAI member. **E** Phase 3: microspar with residual nanoporosity. Ar72, Roana section. RAS member. **F** Phases 1b (arrow) and 3 (microspar with anhedral structures and coalescent morphology). Ar57, Mezzaselva section. RAS member

heterogeneous and contain microaerobic niches. The surroundings of polychaete, oligochaetes and bivalve burrows represent such niches colonized by the meiofauna. These organisms depend on microaerobic conditions (Ott et al. 1982). With gradual lowering of the oxygen content of the bottom waters, the redox potential discontinuity zone rises towards the depositional interface and a corresponding shift in endobenthic tiering is expected (Bromley and Ekdale 1984; Lockair and Savrda 1998).

Following Bromley (1990), if *Chondrites* is found alone and associated with less than 50% bioturbation, it indicates dysaerobic bottom waters. Thus the *Chondrites*-like ichnospecies of our red facies suggest that the red matrices were probably characterized by poor-oxygen environments.

Other macroorganisms construct burrows and feeding tubes which cause chemical and textural heterogeneity in the sediments e.g., sea urchins (De Ridder et al. 1985), bivalves (Gillan and De Ridder 1997). These organisms living in the dysoxic and anoxic sediments take their oxygen in aerobic sediment or in the water and one particularly important consequence of bioturbation is the localized introduction of relatively oxygen-rich bottom water into the sediments (Libes 1992). Chemolithotrophs (Ghiorse 1984) or photoautotrophs (Croal et al. 2004) will colonize the newly formed oxic-anoxic interfaces by living in microaerobic (micro)environments and have a huge potential to catalyze the oxidation of reduced manganese and iron (Fenchel and Finlay 1995). These processes are not applicable to our studied series.

Table 1 Geochemical and isotopic data from the Voltascura (samples 83–117) and Forte Campo di Luserna (samples 146–162) sections

Sample	Colour	$CaCO_3$ (%)	Mg	Fe	Mn	Sr	$\delta^{13}C‰$	$\delta^{18}O‰$
83	G	96.11	2.612	60	669	59	2.34	−1.38
84	G	96.59	2.503	76	411	58	2.10	−1.11
85	G	93.99	2.187	81	907	56	2.46	−2.51
87	G	95.36	2.474	66	411	64	2.56	−0.71
88	G	93.79	2.434	57	796	60	2.27	−2.01
90	G	95.30	1.984	70	1.331	55	2.48	−4.37
91	P	96.77	2.496	86	385	66	2.55	−0.61
92	G	93.90	2.439	108	771	54	2.35	−1.89
93	G	97.35	2.577	105	381	49	2.56	−0.80
95	P	93.44	2.184	76	815	67	3.04	−1.55
97	P	–	–	–	–	–	3.22	−1.34
100	R	95.26	2.185	50	754	50	–	–
106	G	95.03	2.398	110	649	50	2.61	−1.51
115	G	97.79	2.073	64	1.387	47	2.60	−2.54
116	R	92.80	2.738	155	366	71	2.36	−0.56
117	R	88.35	2.661	168	325	81	2.24	−0.77
146	R	95.45	2.954	185	159	78	2.51	−0.66
147	R	95.10	3.039	174	190	76	2.55	−0.54
148	P	96.77	2.847	156	152	79	2.52	−0.59
150	R	96.67	2.877	189	208	69	2.51	−0.62
151	R	95.82	2.756	251	229	70	2.64	−0.83
156	R	91.94	2.217	321	397	68	2.78	−1.49
160	G	98.47	3.330	61	65	260	3.02	−1.14
161	G	98.24	2.941	77	77	271	3.29	−0.97
162	P	96.55	2.223	342	271	67	2.78	−1.37

Second column (colour): G: grey sample, R: red sample, P: pink sample. Trace element columns: Mg, Fe, Mn, Sr in ppm

Summary and conclusion

The succession of sedimentological events in the Ammonitico Rosso sediments can be summarized as follows:

First, a micritic carbonate sediment containing macrofossils (ammonites, bivalves), microfossils (*Protoglobigerina*, *Lenticulina*, radiolarians, coccoliths) and unidentified micritic grains, was deposited on the Trento Plateau. The paleoenvironment was characterized by scarcity or absence of light as indicated by the lack of phototropic algae and corals, scarcity of oxygen recorded by weak bioturbation, and a low sedimentation rate, as indicated by numerous ferruginous hardgrounds and condensed series.

The presence of dysoxic conditions favoured the spread of iron bacterial and fungal biofilms at water–sediment interfaces. They induced the precipitation of iron/manganese oxy-hydroxides leading to the red pigmentation of the micritic matrix. These oxy-hydroxides quickly transformed in hematite (over a period of weeks to months, Cornell and Schwertmann 1996).

The presence of different coloured facies in the RAV is linked to the variation of oxygenation gradients. Bottom oxygenated conditions favoured the spread of burrowers and prevented the development of iron-oxidizing bacterial biofilms (ultimately responsible for hematite) which require a poorly oxygenated environment. As mentioned before, the reddish facies of the RAV are not or only slightly bioturbated, unlike grey facies, where peloidal packstones, indicate higher hydrodynamic energy levels.

The structure of the micrite matrix pertaining to different-coloured samples has been influenced by bacterial filaments in the RAV sediments. Phase 1c, characterized by the occurrence of bacterial mats in the red matrices, prevented the coalescence among crystals, producing subhedral micritic structures. On the contrary, absence of this phase in the greyish facies favoured the fusion of crystals, and the formation of coalescent structures. So, it is possible to argue that there was an organic influence on the successive diagenetic crystal growth, probably up to phase 2c, where relics of bacterial and fungal networks are still visible.

On the other hand, the presence of so-called nanobacteria, abundant on the micritic grains of the red samples, may have had an important role in the biological origin of the initial micrite. Their activity seems to continue up to the formation of microspar when they were probably enclosed by crystal growth.

Micritic diagenesis follows regular steps: first initial micritic crystals (<1 μm) were deposited through chemical precipitation or derived from calcified nanobacteria (sensu Folk 1999). Then, carbonate diagenesis led to the development of incipient neomicrite and neomicrite with

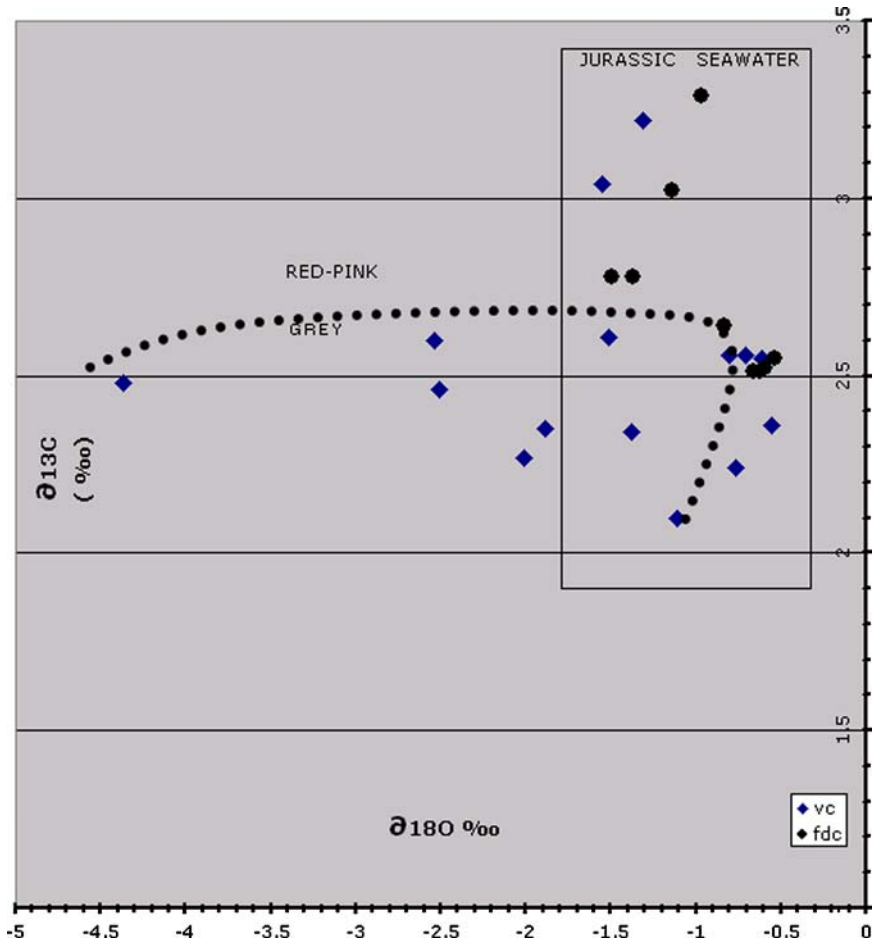

Fig. 11 Scattered diagram showing $\delta^{18}O$ and $\delta^{13}C$ pattern from the Voltascura (diamonds, 'vc') and Forte di Campo Luserna (circles, 'fdc') sections (see Table 1)

interpenetrating textures and amoeboidal morphologies. The final step led to microspar and late cement phases. Interplay of micritic diagenesis and bacterial–fungal activity leads to the different textures and distribution of the reddish pigmentation. This is a relatively common process in numerous Phanerozoic red limestones (Mamet and Préat 2005a,b).

Acknowledgments This research was supported by a postdoctoral fellowship granted to S. Morano from the "Conseil Régional de la Région Bourgogne". The investigations were also supported by the Belgian Fonds National de la Recherche Scientifique (Project FRFC no 2.4509.03) and by the French CNRS (UMR 5561, Biogeosciences). We are grateful to Dr L. Lambert, N. Guichard and Dr R. Romano for experimental help, and to Ms V Mautone for the moral support. We thank the reviewers L. Martire (U. of Turino) and F. Oloritz (U. of Granada) for their constructive remarks.

References

Aller RC (1990) Bioturbation and manganese cycling in hemipelagic sediments. Phil Trans R Soc London A331:51–58

Bosellini A, Martinucci M (1975) Annegamento delle plattaforme carbonatiche. Ann Univ Ferrara IX 5 10:181–193

Bosellini A, Winterer EL (1975) Pelagic limestones and radiolarites of the Tethyan Mesozoic: A genetic model. Geology 3:279–282

Boulvain F (1993) Sédimentologie et diagenèse des monticules micritiques 'F2j' du Frasnien de l'Ardenne. Serv Géol Belgique Prof Paper 260, pp 427

Boulvain F, De Ridder Ch, Gillan D, Mamet B, Préat A (2001) Iron microbial communities in Belgian Frasnian carbonate mounds. Facies 44:47–60

Brierley CL (1990) Metal immobilization using bacteria. In: Ehrlich HL, Brierley CL (eds) Microbial mineral recovery. McGraw-Hill, New York, pp 303–324

Bromley RG (1990) Trace fossils. Biology and taphonomy. Unwin Hyman, London, pp 280

Bromley RG, Ekdale AA (1984) *Chondrites*: a trace fossil indicator of anoxia in sediments. Science 224:872–874

Caracuel JE, Olóriz F, Sarti C (1997) Environmental evolution during the Late Jurassic at Lavarone (Trento Plateau, Italy). Palaeogeogr Palaeoclimatol Palaeoecol 135:163–177

Catullo TA (1853) Intorno a una nuova classificazione delle calcarie rosse ammonitiche delle Alpi Venete. Mem Real Istit Veneto Let Arti 5:1–57

Clari P, Martire L (1996) Interplay of cementation, mechanical compaction, and chemical compaction in nodular limestones of the Rosso Ammonitico Veronese (Middle-Upper Jurassic, Northeastern Italy). J Sediment Res 66:447–458

Clari P, Marini P, Pastorini M, Pavia G (1984) Il Rosso Ammonitico inferiore (Baiociano-Calloviano) nei Monti Lessini settentrionali (Verona). Riv Ital Paleont Stratigr Milano 90:15–86

Cornell RM, Schwertmann U (1996) The iron oxides: structure, properties, and uses. Wiley-VCH Weinhein, Germany, p 664

Courties C, Vaquer A, Troussellier M, Chretiennot-Dinet MJ, Neveux J, Machado MC, Claustre H (1994) Smallest eukaryotic organism. Nature 370:255

Croal LR, Johnson CM, Beard BL, Newman DK (2004) Iron isotope fractionation by Fe(II) oxidizing photoautrophic bacteria. Geochim Cosmochim Acta 68:1227–1242

De Ridder C, Jangoux M, De Vos L (1985) Description and significance of a peculiar intradigestive symbiosis between bacteria and a deposit-feeding echinoid. J Exp Mar Biol Ecol 96:65–75
De Zigno A (1850) Coup d'oeil sur les terrains stratifiés des Alpes Vénétiennes. Naturw Abh 4:1–16 Wien
Fenchel T, Finlay J (1995) Ecology and Evolution in Anoxic Worlds. Oxford Series in Ecology and Evolution, Oxford University Press, Oxford, UK, pp 276
Folk RL (1999) Nanobacteria and the precipitation of carbonate in unusual environments. Sediment Geol 126:47–55
Gaetani M (1975) Jurassic stratigraphy of the Southern Alps: a review. In: Squires C (ed) Geology of Italy: Lybian Arab Republic. Earth Science Society, Tripoli, pp 377–402
Ghiorse WC (1984) Biology of iron and manganese-depositing bacteria. Ann Rev Microbiol 38:515–550
Gillan D, De Ridder C (1997) Morphology of ferric iron-encrusted biofilm forming on the shelf of a burrowing bivavle (Mollusca). Aquat Microb Ecol 12:1–10
Hendry JP (1993) Calcite cementation during bacterial manganese, iron and sulphate reduction in Jurassic shallow marine carbonates. Sedimentology 40:87–106
Jenkyns HC, Clayton CJ (1986) Black shales and carbon isotopes in pelagic sediments from the Tethyan Lower Jurassic. Sedimentology 33:87–106
Libes SM (1992) An introduction to marine biogeochemistry, Wiley, New York, pp 734
Lockair RE, Savrda CE (1998) Ichnofossil tiering analysis of a rhythmically bedded chalk-marl sequence in the Upper Cretaceous of Alabama. Lethaia 31:311–322
Loreau JP (1972) Pétrographie de calcaires fins au microscope électronique à balayage: introduction à une classification des ≪micrites≫. CR Acad Sci Paris 274:810–813
Machel HG (1999) Application of cathodoluminescence to carbonate diagnesis. In: Pagel M, Barbin, V, Blanc P, Ohnensletter D (eds) Cathodoluminescence in Geosciences. Springer-Verlag, Berlin, pp 271–301
Mamet B, Préat A (2003) Sur l'origine bactérienne et fongique de la pigmentation de l'Ammonitico Rosso (Jurassique, région de Vérone, Italie du nord). Rev Micropal 46:35–46
Mamet B, Préat A (2005a) Why is 'red marble' red? Rev Espan Micropal 37:13–21
Mamet B, Préat A (2005b) Iron-bacterial mediation in phanerozoic red limestones. State of the Art. Sed Geol (in press)
Martire L (1988) Età, dinamica deposizionale e possibile organizzazione sequenziale del Rosso Ammonitico dell'Altopiano di Asiago (VI). Rendiconti Soc Geol Ital 11:231–236
Martire L (1989) Analisi biostratigrafica e sedimentologica del Rosso Ammonitico Veronese dell'Altopiano di Asiago (VI). Ph.D. Thesis, University of Torino, p 166
Martire L (1992) Sequence stratigraphy and condensed pelagic sediments. An example from the Rosso Ammonitico Veronese, northeastern Italy. Palaeogeogr Palaeoclimatol Palaeoecol 94:169–191
Martire L (1996) Stratigraphy, facies and synsedimentary tectonics in the Jurassic Rosso Ammonitico Veronese (Altopiano di Asiago, NE Italy). Facies 35:209–236
Martire L, Clari PA, Pavia G (1991) Il significato stratigrafico della sezione di Cima Campo di Luserna (Giurassico delle Alpi Meridionale, Italia nord orientale). Palaeopelagos 1:56–65
Megonigal JP, Hines ME, Visscher PT (2003) Anaerobic metabolism: linkages to trace gases and aerobic processes. In: Schlesinger W, Holland HD, Turekian B (eds) Treatise on geochemistry, biogeochemistry. Elsevier, Amsterdam 8:317–424
Munn CB (2004) Marine microbiology. Ecology and application. Garland Science/Bios Scientific, Oxford, UK, pp 282
Munnecke A, Westphal H, Reijmer JJG, Samtleben C (1997) Microspar development during early marine burial diagenesis: a comparison of Pliocene carbonates from the Bahamas with Silurian limestones from Gotland (Sweden). Sedimentology 44:977–990
Ott JA, Rieger G, Rieger R, Enderes F (1982) New mouthless interstitial worms from the sulfide system: symbiosis with prokaryotes. PSZNI Mar Ecol 38:313–333
Powell E (1989) Oxygen sulfide and diffusion: why thiobiotic meiofauna must be sulfide-insensitive first-order respires. J Mar Res 47:887–932
Préat A, Cauet S, Herbosch A (1983) Caractère épigénétique-étranger des gîtes filoniens Pb-Zn (Ba-F) du district du bord sud du Synclinorium de Dinant (Belgique). Mineral Depos 18:349–363
Préat A, Mamet B, Bernard A, Gillan D (1999) Bacterial mediation red matrices diagenesis, Devonian, Montagne Noire (Southern France). Sediment Geol 126:223–243
Sarti C (1985) Biostratigraphie et faune à ammonites du Jurassique supérieur de la plate-forme atésine (Formation du Rosso Ammonitico Véronais). Rev Paléobiol 4:321–330
Sarti C (1986) Fauna e biostratigrafia del Rosso Ammonitico del Trentino centrale (Kimmeridgiano-Titoniano). Boll Soc Paleontol Ital 23:473–514
Sarti C (1993) Il Kimmeridgiano delle Prealpi Veneto-Trentine: Fauna e Biostratigrafia. Mem Mus Civ Stor Nat Verona (II Ser) Sez Sc Terra 5:145
Schulz HD (2000) Quantification of early diagenesis; dissolved constituents in marine pore water. In: Schulz HD, Zabel M (eds) Marine Geochemistry. Springer-Verlag, Berlin, pp 85–128
Scudeler Baccelle L, Nardi S (1991) Interaction between calcium carbonate and organic matter: An example from the Rosso Ammonitico Veronese (Veneto, north Italy). Chem Geol 93:301–311
Sethmann I, Neuweiler F, Geipel G (2001) Comparative fluorescence characteristics of the Calcari grigi Formation and the Rosso Ammonitico Veronese (Jurassic, Trento Platform, Northern Italy): significance for palaeobathymetry and petrogenesis. 21st IAS-Meeting of Sedimentology 3–5 September 2001 Davos Switzerland
Stolp H (1988) Microbial ecology: organisms, habitats, activities. Cambridge sudies in ecology. Cambridge University Press, Cambridge, UK, p 308
Sturani C (1964) La Successione delle Faune ad Ammoniti nelle Formazioni mediogiurassiche delle Prealpi venete Occidentale. Mem Inst di Geol i Mineral Univ di Padova 24:1–63
Sturani C (1971) Ammonites and stratigraphy of the *Posidonia alpina* beds in the Venetian Alps (Middle Jurassic, mainly Bajocian). Mem Inst Geol Min Univ Padova 28:1–190
Tobin KJ, Walker K (1996) Ordovician low-to-intermediate Mg calcite marine cements from Sweden: marine alteration and implications for oxygen isotopes in Ordovician seawater. Sedimentology 43:719–735
Van den Hoek C, Mann DG, Jahns HM (1995) Algae, an introduction to phycology. Cambridge University Press, Cambridge, UK, pp 623
Wachter E, Hayes JM (1985) Exchange of oxygen isotopes in carbon-dioxide-phosphoric acid systems. Chem Geol 52:365–374
Winterer EL, Bosellini A (1981) Subsidence and sedimentation on a Jurassic passive continental margin, Southern Alps, Italy. AAPG Bull 65:394–422
Winterer EL, Metzler CV, Sarti M (1991) Neptunian dykes and associated breccias (Southern Alps, Italy and Switzerland): role of gravity sliding in open and closed systems. Sedimentology 38:381–404
Zempolich WG (1993) The drowning succession in Jurassic carbonates of the Venetian Alps, Italy: a record of supercontinent breakup, gradual eustatic rise, and eutrophization of shallow-water environments. AAPG Mem 57:63–105